Environmental Pollution 344 (2024) 123306

Contents lists available at ScienceDirect

Environmental Pollution

journal homepage: www.elsevier.com/locate/envpol

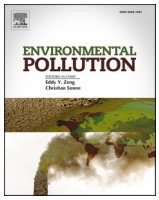

Fine particle pollution during megafires contains potentially toxic elements☆

Raissa L. Gill [a,b,*], Robert Fleck [b], Ky Chau [b], Mika T. Westerhausen [c], Thomas E. Lockwood [c], Jake P. Violi [d], Peter J. Irga [e], Martina A. Doblin [a,f], Fraser R. Torpy [b]

[a] Productive Coasts, Climate Change Cluster, University of Technology Sydney, Ultimo, NSW, 2007, Australia
[b] Plants and Environmental Quality Research Group, School of Life Sciences, University of Technology Sydney, Ultimo, NSW, 2007, Australia
[c] Hyphenated Mass Spectrometry Laboratory, School of Mathematical and Physical Sciences, University of Technology Sydney, Ultimo, NSW, 2007, Australia
[d] School of Chemistry, University of New South Wales, Sydney, NSW, 2052, Australia
[e] Plants and Environmental Quality Research Group, School of Civil and Environmental Engineering, University of Technology Sydney, Ultimo, NSW, 2007, Australia
[f] Sydney Institute of Marine Science, Mosman, NSW, 2088, Australia

ARTICLE INFO

Keywords:
Aerosols
Air quality
Biomass burning
Filter forensics
Solubility
Source apportionment

ABSTRACT

Wildfires that raged across Australia during the 2019–2020 'Black Summer' produced an enormous quantity of particulate matter (PM) pollution, with plumes that cloaked many urban centres and ecosystems along the eastern seaboard. This has motivated a need to understand the magnitude and nature of PM exposure, so that its impact on both built and natural environments can be more accurately assessed. Here we present the potentially toxic fingerprint of PM captured by building heating, ventilation, and air conditioning filters in Sydney, Australia during the peak of the Wildfires, and from ambient urban emissions one year later (Reference period). Atmospheric PM and meteorological monitoring data were also assessed to determine the magnitude and source of high PM exposure. The wildfires were a major source of PM pollution in Sydney, exceeding the national standards on 19 % of days between November–February. Wildfire particles were finer and more spherical compared to Reference PM, with count median diameters of 892.1 ± 23.1 versus 1484.8 ± 96.7 nm (mean ± standard error). On an equal-mass basis, differences in potentially toxic elements were predominantly due to higher SO_4^{2-}-S (median 20.4 vs 4.7 mg g^{-1}) and NO_3^--N (2.4 vs 1.2 mg g^{-1}) in Wildfire PM, and higher PO_4^{3-}-P (10.4 vs 1.4 mg g^{-1}) in Reference PM. Concentrations of remaining elements were similar or lower than Reference PM, except for enrichments to F^-, Cl^-, dissolved Mn, and particulate Mn, Co and Sb. Fractional solubilities of trace elements were similar or lower than Reference PM, except for enhanced Hg (12.1 vs 1.0 %) and greater variability in Cd, Hg and Mn solubility, which displayed upper quartiles exceeding that of Reference PM. These findings contribute to our understanding of human and ecosystem exposures to the toxic components of mixed smoke plumes, especially in regions downwind of the source.

1. Introduction

Climate change is associated with conditions more favorable for wildfires in many locations by acting on drivers of heat and water availability in the atmosphere and terrestrial landscape (Aldersley et al., 2011; Pechony and Shindell, 2010). Increasing wildfire frequency and severity have already been observed in many regions, including the recent megafires in Australia, Brazil, California, and Russia (Bowman et al., 2020; Huang et al., 2015). Australia is acknowledged as the most fire-prone continent due to the high fuel load associated with its endemic eucalypt forests (Boer et al., 2020) and the propensity for fuel dryness, due to the continent's high solar radiation, low relative humidity, and prolonged drought periods (Nolan et al., 2016). During spells of hot, dry, and windy weather, these conditions enable wildfires (known locally as bushfires) to spread quickly across a highly flammable landscape. The 2019–2020 Black Summer Wildfires were an extreme instance, burning 30.4 Mha of land (Borchers Arriagada et al., 2020) with substantial impacts to both human (Borchers Arriagada et al., 2020; Johnston et al., 2021) and animal (Ward et al., 2020) morbidity and mortality. Furthermore, the vast quantity of particulate matter (PM) emitted into the atmosphere (Hirsch and Koren, 2021; van der Velde

☆ This paper has been recommended for acceptance by Admir Créso Targino.

* Corresponding author. PO Box 123, Ultimo, NSW, 2007, Australia.
E-mail address: raissa.gill@uts.edu.au (R.L. Gill).

https://doi.org/10.1016/j.envpol.2024.123306
Received 29 August 2023; Received in revised form 4 January 2024; Accepted 4 January 2024
Available online 5 January 2024

Abbreviations

AHU = air handling unit
CMD = count median diameter
ESD = equivalent spherical diameter
FF = filter forensics
HVAC = heating, ventilation, and air conditioning
PM = particulate matter
$PM_{0.1}$ = ultra-fine particulate matter with aerodynamic diameter ≤0.1 μm
PM_1 = submicron particulate matter with aerodynamic diameter ≤1 μm, includes $PM_{0.1}$
$PM_{2.5}$ = fine particulate matter with aerodynamic diameter ≤2.5 μm, includes PM_1
PM_{10} = particulate matter with aerodynamic diameter ≤10 μm, includes $PM_{2.5}$
PM_{25} = particulate matter with aerodynamic diameter ≤25 μm, includes PM_{10}
PTE = potentially toxic element
TSP = total suspended particles

et al., 2021) can travel great distances downwind from active fire locations (Peterson et al., 2021), impacting humans and biota distant from the source.

During a wildfire, the primary route of PM exposure for humans is inhalation. Its toxicity in mammals is attributed to large quantities of deeply inhalable fine particulates ($PM_{2.5}$ - aerodynamic diameter ≤2.5 μm), the dominant size fraction of pyrogenic PM (Reid et al., 2005). This fraction not only penetrates the gas exchange region of the respiratory tract (Miller et al., 1979; Pinkerton et al., 2000), but the ultrafine portion ($PM_{0.1}$ - aerodynamic diameter ≤0.1 μm) can cross the alveolar-capillary membrane, where it circulates in the blood (Nemmar et al., 2002). Toxicity may act on cell viability, cell apoptosis, inflammation, oxidative stress, and genotoxicity (Dong et al., 2017), leading to adverse respiratory and cardiovascular health effects (Reid et al., 2016). Regional estimates during the 2019–2020 Black Summer attributed 417 mortalities and 4456 hospitalisations to wildfire PM exposure (Borchers Arriagada et al., 2020). While PM quantity and size are key causative factors for adverse health outcomes during wildfire, recent evidence suggests that wildfire $PM_{2.5}$ may be more toxic than equal doses of ambient $PM_{2.5}$ (Aguilera et al., 2021; Franzi et al., 2011; Wegesser et al., 2009). This is especially important for water-soluble elements, as they possess higher bioavailability and may cause greater injury compared to their insoluble counterparts (Costa and Dreher, 1997).

Given the magnitude of PM pollution during the 2019–2020 Wildfires, there was also significant likelihood for ecotoxicological effects to occur upon the PM's deposition. Acidic compounds like sulfates and nitrates which are associated with secondary aerosol formation during transport (Akagi et al., 2011; Li et al., 2015) can reduce the calcium and dissolved organic carbon content of soils that lack sufficient buffering, leading to reduced plant growth and mortality (Battles et al., 2014; Monteith et al., 2007). In aquatic systems, the deposition of smoke-derived metals like copper (Sparks and Wagner, 2021) can have toxic effects on marine phytoplankton (Paytan et al., 2009), with implications for grazing and bioaccumulation in marine food webs. While nutrient enrichment has been observed in ocean waters surrounding Australia during wildfires (Li et al., 2021; Tang et al., 2021), deposition-induced ecotoxicity has been insufficiently studied, especially given that observations in both terrestrial and aquatic environments closer to the source of fires are very limited.

The highly unpredictable and dangerous nature of wildfires presents a unique set of challenges for collecting representative PM samples, so observations that capture the fingerprint of wildfire-influenced plumes are highly valuable for informing their potential impacts. Given the longevity and reach of megafire plumes like those observed during the 2019–2020 Black Summer (Peterson et al., 2021), examining aged PM that has undergone atmospheric processing and mixing is imperative due to its influence on particle size and composition (Kanakidou et al., 2005) as well as its relevance for human exposure in urban centres. Here we gathered a retrospective, four-month sample of PM in Sydney's Central Business District (CBD) immediately after the Black Summer Wildfires and from ambient urban emissions one year later for comparison. This study uniquely describes PM to which Australia's largest urban population was exposed during the 2019–2020 fires, as well as providing previously undocumented atmospheric concentration analyses, source apportionment, particle size distributions, and dissolved and particulate fractions of potentially toxic trace elements and ions (PTEs) listed in Australia's National Pollutant Inventory (Department of the Environment, 2015). We anticipated that because of its mixed pyrogenic and urban origin, analysis of the PM fingerprint would reveal size distributions and elemental concentrations that deviated strongly from ambient urban emissions.

2. Material and methods

2.1. Study site

The study site (33.8832° S, 151.2005° E, University of Technology Sydney (UTS) Ultimo campus) is in Sydney's CBD, the most populated city in Australia (5.3 million in 2022) (Australian Bureau of Statistics, 2023). Sydney is situated in a low-lying basin between the eastern seaboard and large areas of sclerophyll forest, acting as a natural trap for fine PM pollution due to natural geographic and meteorological conditions that hold PM within the basin (Cohen et al., 2011). Sydney's climate is classified as temperate with no dry season and hot summers (Cfa Köppen-Geiger classification) (Beck et al., 2018). During the Summer months, local sources of fine particles are predominantly coal-burning power generation and diesel vehicles (50–70 %), as well as industrial sources (30–50 %) (Cohen et al., 2016). Coarser particles include soil, sea-spray, and industrial activities (Cohen et al., 2016).

2.2. Sample collection

Building heating, ventilation, and air conditioning (HVAC) filters were used to collect and extract PM arriving in Sydney's CBD during the peak of the Black Summer Wildfires (Mahdavi and Siegel, 2020). The strength of this approach is its ability to bulk-capture PM without *a priori* notice of catastrophic events such as wildfires and was used here to collect sufficient mass for both this study and ongoing experimentation. The analysis of HVAC-derived PM, known as filter forensics (FF), yields a spatially and temporally integrated sample that is indicative of exposure across a broader sampling region and period. This is advantageous when sampling densely concentrated plumes of variable source location or conditions, as these may provide a skewed snapshot of the aerosol(s) of interest. FF yields relatively similar trace element concentrations (Mahdavi et al., 2021) and size distributions for particles spanning 1–10 μm (Mahdavi et al., 2021; Mahdavi and Siegel, 2020), with limited evidence of ongoing chemical transformation on the filter surface after its deposition (Weschler and Nazaroff, 2010; Xu et al., 2015). For particles <1 μm, the limit of detection varies amongst studies, though sizes down to 0.45 μm have been achieved (Dev et al., 2022; Mahdavi et al., 2021; Mahdavi and Siegel, 2020; Stephens and Siegel, 2012). More information on the representativeness of FF sampling can be found in the Supplementary Material (Text S1).

Building HVAC filters were retrieved from two mechanically ventilated, adjoined buildings (Central Buildings 4 and 7), each featuring an independent centralised HVAC system with either south-west (CB4) or north-west (CB7) facing air intake ducts. Both buildings drew outdoor air into their respective air handling unit (AHU) through straight

ducting, where it was filtered directly by one of several primary HVAC filters before being secondarily filtered for indoor circulation. Filters are replaced on a four-month rotation. HVAC filters from CB4 (n = 12) and CB7 (n = 9) AHUs were in service for 120 days during the peak of the Wildfires (1 November 2019 – 28 February 2020; Fig. S1A). Given that PM from the two buildings featured similar particle size distributions (two-sample z-test: $p = 0.240$) and chemical composition (PERMANOVA: $p = 0.227$; PERMDISP: $p = 0.821$), these samples were analysed collectively. HVAC filters were also retrieved one year later from Building 4 AHU (n = 12) as a Reference for ambient urban PM (2 November 2020 – 1 March 2021; Fig. S1B). Building HVAC operative settings were kept consistent between study periods and AHUs.

All filters were 594 × 594 mm Aeropleat III MERV 8 type (Camfil, Sweden) with a pleat depth of 44 mm (filter airflow rate: 3400 $m^3\ h^{-1}$) and a clean-filter, minimum efficiency reporting value (MERV) of ≥70 % for $PM_{3\text{-}10}$ and ≥20 % for $PM_{1\text{-}3}$. In practice, runtime increases filtration efficiency whereby captured PM acts as a secondary layer for particle interception and impaction, increasing the effectiveness of $PM_{0.1\text{-}0.3}$ capture by up to 80 % (Alavy and Siegel, 2020; Hanley et al., 1994). To control for the extraction process, four unused filters of identical grade, material, and supplier were also sampled and analysed (Procedural control; Fig. S1C).

2.3. Sample extraction

PM was extracted from the filters using a similar methodology to Mahdavi and Siegel (2020). Briefly, a vacuum sampler was constructed by fitting polyvinyl tubing (8 mm) either side of a sealed cassette which housed a mixed cellulose ester filter (37 mm, pore size 0.8 μm) backed with a cellulose pad (ZEF728MCE; Zefon International, USA). One end of the sampler was encased with a 25 μm pre-screen (XTRECHT03; Allied Filter Fabrics, Australia) as an exclusionary mechanism for HVAC filter fibers and particles ≥25 μm. The other end was connected to a vacuum with an unobstructed inlet flow rate of 100 L min^{-1} (pressure −70 to −90 kPa). For each extraction, the HVAC filter mesh was removed from its frame with non-metal tools. Sealed cassettes were weighed prior to sampling using an analytical balance (A200S; Sartorius, Germany) and fitted to the vacuum sampler. The head of the sampler was held flat against the filter mesh and vacuumed whilst moving horizontally across the filter pleats. This was repeated three times along each pleat to increase particle recovery. The sampler headpiece was periodically cleared of larger material to ensure unobstructed vacuum pressure, and the sealed cassette was changed when suction diminished. To avoid contamination between HVAC filters, the entire assembly (tubing, cassette, and pre-screen) was replaced between each filter. Extracted mass was calculated by subtracting the initial and post-collection weights of the sealed cassette under standardised conditions. PM analyses were conducted on a subset of extracted mass.

2.4. Sample processing

To prepare samples for analysis, loose PM within the cassettes was carefully transferred into sterile 50 mL centrifuge tubes (Falcon, USA) by rinsing three times with fresh Milli-Q water (18.2 Ω; Millipore, Germany). The filter paper containing embedded PM was placed in the tube using acid-washed plastic forceps. Tubes were then topped up to 50 mL with Milli-Q, sealed, shaken, and left for 20 min. To extract embedded PM from the cassette filters, the solutions were sonicated for 15 min. Pilots indicated that this was sufficient to remove the majority of mass without filter destruction, with only 4.2 ± 1.3 % mean ± standard deviation (sd) remaining in the filter (n = 9). Sonicated cassette filters were then transferred to a new centrifuge tube, and the remaining particulate material separated through centrifugation (23 °C for 15 min at 7.826 g) (Model 5404; Eppendorf AG, Germany). The liquid filtrate was carefully removed for dissolved analyses, leaving behind a firm pellet for the particulate fraction. The dissolved fraction was further filtered through a sterile, pre-flushed 0.22 μm pore size polyethersulfone membrane syringe filter (Millex-GP Filter; Millipore, Germany). Several aliquots of the dissolved and particulate fractions were set aside for downstream processing, with the cassette filter preserved for trace elements. Extracts were stored at −80 °C until analysis. Prior to analysing samples, particulate extracts were verified gravimetrically to account for potential particle losses during sample extraction, storage, and processing. Recoveries were 99.0 ± 4.6 % (mean ± sd) of initial post-extraction weights. Sample weights were adjusted accordingly prior to mass correction.

2.5. Airborne concentration and source analyses

Atmospheric PM and meteorological data recorded at the nearest air monitoring station (4 km away) in Rozelle (33.8658° S, 151.1625° E) were obtained from the NSW air quality monitoring network (Climate and Atmospheric Science Branch, Department of Planning and Environment, 2023; Riley et al., 2020). Hourly and daily-mean measurements spanning pre- to post-HVAC sampling (1 May 2019 – 1 May 2021) were retrieved for the following variables: $PM_{2.5}$, PM_{10}, wind direction, wind speed, temperature, relative humidity, rainfall, solar radiation. Rozelle and the HVAC sampling location are located 0.7–1 km away from high-density traffic at an elevation of 22 and 26.7 m respectively. Traffic count data recorded from the nearest sensor on Parramatta Road (#19065, 33.887417° S, 151.173325° E) were retrieved from the NSW Traffic Volume Viewer (Transport for NSW, 2023). Mean daily counts for each month during the Wildfire and Reference periods were obtained for both eastbound and westbound traffic. This station is located approximately 3 km away from both HVAC and Rozelle sites on the main arterial road that would influence traffic-related air pollution at these locations.

The importance of local versus remote sources of PM pollution were assessed using polar plots in the openair package (Carslaw and Ropkins, 2012) for R V4.2.1 (R Core Team, 2022). These were configured to a conditional probability function (CPF) set to national standards of 50 μg m^{-3} PM_{10} and 25 μg m^{-3} $PM_{2.5}$ (Department of the Environment and Heritage, 2005). This analysis partitions the probability of exceeding these concentrations by wind direction and speed, and is indicative of the direction and proximity of source(s) contributing to local concentrations (Uria-Tellaetxe and Carslaw, 2014). This analysis was supplemented by Hybrid Single-Particle Lagrangian Integrated Trajectory (HYSPLIT) modelling using the NOAA Air Resources Laboratory web-based system (V5.2.0) (Rolph et al., 2017; Stein et al., 2015) to generate air mass back-trajectories and identify possible source regions. Initial air parcels were generated at 00:00 on the 1st of November 2019 (UTC). These were run backwards in time for 72 h each, with new trajectories released every 6 h across the 4-month wildfire sampling window. All air parcels arrived at the HVAC sampling location (33.8832° S, 151.2005° E) at an altitude 0.5 times the planetary boundary level (PBL) to ensure trajectories did not fall prematurely out of suspension. HYSPLIT was driven by 6-hourly meteorological data from NOAA's Global Forecast System (GFS) at a spatial resolution of 0.25° (approximately 25 km^2). Regions associated with national standard exceedances (>50 μg m^{-3} PM_{10} and >25 μg m^{-3} $PM_{2.5}$) were calculated using gridded percentile differences in the trajLevel function of the openair package (Carslaw and Ropkins, 2012) for R (R Core Team, 2022). To aid interpretations, confirmed fire locations recorded throughout the 2019–2020 Black Summer, including single fires or the perimeters of burnt zones, were obtained from the National Indicative Aggregated Fire Extent Dataset (Department of Climate Change, Energy, the Environment and Water, 2020) and visualised in R (R Core Team, 2022) using the ggplot2 (Wickham, 2016), ggspatial (Dunnington, 2023), ozmaps (Sumner, 2021), sf (Pebesma, 2018), and shapefiles (Stabler, 2022) packages.

2.6. Particle size and morphology

Particle size analysis was conducted using a Cytoflex LX flow cytometer (C40321; Beckman Coulter, USA) operated using CytExpert software (V2.1; Beckman Coulter, USA). Samples were prepared by resuspending the particulate extracts in Milli-Q and combining with the dissolved fraction (1:1 ratio) following 10 min sonication. Samples were analysed after vortexing (30 s) to determine particle count and equivalent spherical diameters (ESD). Milli-Q blanks were run between each sample until events read <100 μL^{-1} min^{-1}. Solutions were diluted 1:2 with Milli-Q and re-analysed if the abortion rate was ≥2.5 %. Particle aggregates were assessed by plotting FSC-H × FSC-A and checking for linear correspondence (deviation from linearity indicating aggregate presence; $R^2 > 0.99$). For calibration, six suspensions of non-fluorescent polystyrene microspheres (Flow Cytometry Size Calibration Kit; Thermofisher, USA) of known diameters (1–15 μm) were prepared as above in Milli-Q (linear calibration of FSC-A × SSC-A: $R^2 > 0.99$). All data were processed in FlowJo software (V10.8.1; BD, USA). Specific instrument parameters and settings can be found in the Supplementary Material (Table S1).

To examine particle morphology, composite samples from three individual cassettes (1:1:1 mass ratio) were imaged using a field emission scanning electron microscope (SEM) with the GEMINI column (Supra 55VP; Carl Zeiss, Germany). Images were taken at a 5 kV accelerating voltage to improve imaging of fine carbonaceous particles, at 100–500× magnification.

2.7. Potentially toxic elements

Major ion analyses were performed on a subset of the Wildfire and Reference sample extracts using high-pressure ion chromatography (Integrion HPIC; Thermofisher, Australia). Dissolved sample aliquots were diluted 1:10 to 1:50 with Milli-Q to avoid swamping the chromatograph. The mass concentrations of the following PTEs (and Na^+) were determined: Cl^-, F^-, Na^+, NH_4^+-N, NO_2^--N, NO_3^--N, PO_4^{3-}-P, SO_4^{2-}-S. Six-point calibration curves (0.01–20 ppm) were prepared from mixed single element standards (TraceCERT; Sigma-Aldrich, Australia) in Milli-Q.

Trace element (TE) analysis was performed on dissolved, particulate and filter extracts using solution nebulization inductively coupled plasma mass spectrometry (SN ICP-MS; 7700x series; Agilent, Australia). Particulate and filter samples were vacuum dried overnight, then digested in 1:1 69 % HNO_3/34 % HCl and made to volume with Milli-Q. Dissolved samples were digested in 3 % HNO_3/1 % HCl. Samples were diluted 1:100 to 1:3000 with Milli-Q before running on SN-ICP-MS to ensure they fell within calibration. The mass concentrations of the following PTEs were determined: As, B, Be, Cd, Co, Cr, Cu, Hg, Mn, Ni, Pb, Sb, Se and Zn. Calibration points spanned twelve concentrations (0–5 ppm) and was prepared from a 68-elemental standard (ICP-MS68A-500; Choice Analytical, Australia) in a mixture of 2 % HNO_3/1 % HCl (Seastar Baseline®; Choice Analytical, Australia). An online internal standard of 100 ppb Rhodium solution in 2 % HNO_3/1 % HCl was used to normalise matrix effects.

Quality control involved running blanks, duplicate PM samples (n = 3), mixed calibration standards and/or Certified Reference Material (NCS DC 73016a and NCS ZC 71008; NCS Testing Technology Co, China) every 15–25 reads. Blanks read low and stable (ions <0.05 ppm and TEs <10 ppb), duplicate variance was within ±5 (ions) or ±10 (TEs) %, and recoveries were within 94–111 % of expected values for all PTEs listed, except B and Se (excluded from further analysis). Specific HPIC and SN ICP-MS parameters can be found in the Supplementary Material (Tables S2 and S3).

2.8. Data analysis

For airborne analyses, differences in PM concentration and meteorology between the two study periods were assessed separately by Permutational Analysis of Variance (PERMANOVA) on a Euclidean distance matrix with 999 permutations. Daily mean traffic counts across all months/directions spanning the two study periods were assessed by Analysis of Variance (ANOVA). The proportion of $PM_{2.5}$ mass within PM_{10} was calculated from daily mean mass concentrations (μg m^{-3}) for both study periods and expressed as a percentage. Comparisons were performed using PERMANOVA.

For size analyses, overall differences in the particle number distributions between the two periods were assessed by a two-sample z-test. Individual particles of varying ESDs were allocated to the appropriate size fraction (<PM_{10}, $PM_{2.5\text{-}10}$ <$PM_{2.5}$, <PM_1, $PM_{0.1\text{-}1}$, <$PM_{0.1}$), standardised to analysed sample mass, and used to calculate the proportion of particles falling within various size fractions. The latter was calculated from binned particle counts standardised to PM mass (number of particles μg^{-1}) and is expressed as a percentage for both study periods. Count median diameters (CMD) were calculated as the median ESD of particles within a given size fraction. Individual PERMANOVAs were used for size metric comparisons.

For chemical analyses, procedural control data were first subtracted from concentrations of both study periods to remove contributions from the extraction process. Given that PM extractions from the HVAC filter mesh were not 100 % efficient, and we did not have the means to quantify infiltration rate through the building envelope, PTE concentrations were standardised by analysed PM mass (μg g^{-1} PTE in PM) as opposed to air volume and pollutant loading (μg m^{-3} PTE in air). The fractional solubility of each trace element was expressed as a percentage of analysed sample mass. To assess differences in the overall chemical composition between the two study periods, the concentration matrix comprised of all PTEs were compared by PERMANOVA and Permutational Multivariate Analysis of Dispersion (PERMDISP - analogous to Levene's test for equality of variance). Elements that contributed the most to these differences were then identified by the magnitude of vectors in Principal Components Analysis (PCA), which was calculated based on Euclidean distance of the standardised concentration matrix (μg g^{-1} PTE in PM) and visualised on a −1 to 1 biplot. Compositional data were summarised by medians and lower/upper quartiles (q_1–q_3) as many elements had skewed distributions. Individual differences for each PTE were tested by PERMANOVA and PERMDISP as appropriate. Pearson correlations between Na^+ and Pb were used to assess potential associations with sea salt and anthropogenic sources, respectively.

All data analysis and visualization were performed in R (R Core Team, 2022) using the following packages: BDSA (Arnholt and Evans, 2021), dplyr (Wickham et al., 2022), ggplot2 (Wickham, 2016), ggpubr (Kassambara, 2020), and vegan (Oksanen et al., 2022).

3. Results and discussion

3.1. Particle pollution in Sydney's CBD during the Black Summer Wildfires

Throughout the 2019–2020 Black Summer, wildfires burned across the entire continent, including locations to the north, south and west of Sydney's CBD (Fig. 1A). The fires emitted burnt vegetation, smoke, and surface soil entrained during pyro-convection into the atmosphere (Gaudichet et al., 1995; Wagner et al., 2018); these PM-rich plumes were then carried by winds to Sydney, mixing with urban particles and impacting the air quality of Australia's largest human population.

Daily PM concentrations at the Rozelle monitoring station, located 4 km away from the HVAC units where PM was sampled, exceeded the national standards (50/25 μg m^{-3} $PM_{10}/PM_{2.5}$) (Department of the Environment and Heritage, 2005) on 19 % of days over the four-month sampling period. Exceedances occurred most frequently during higher velocity (6–8 m s^{-1}) south-westerly winds (Fig. 1B), indicating that a substantial portion of particles in the Wildfire samples were attributable to remote sources, rather than local anthropogenic sources. Regional

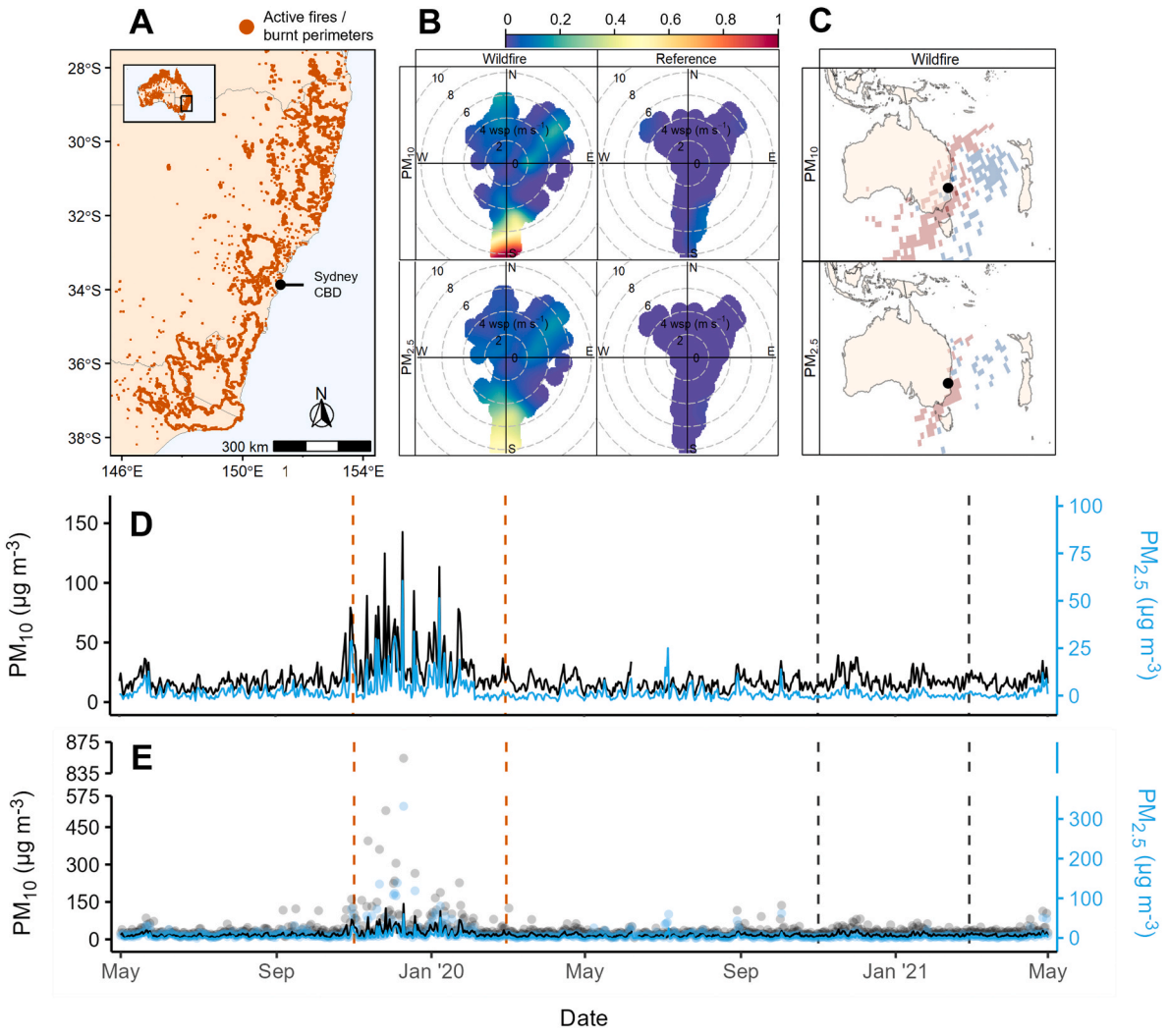

Fig. 1. Airborne concentration and source analysis of PM pollution in Sydney's CBD during the 2019–2020 Black Summer Wildfires and 2020–2021 Reference period. A) depicts location of HVAC sampling relative to confirmed fire cases (orange points as single fires or perimeters of burnt zones); B) polar plots for the two study periods (Wildfire and Reference) by pollutant (PM_{10} and $PM_{2.5}$), where colour denotes the probability of exceeding hourly concentrations of 50 µg m^{-3} PM_{10} and 25 µg m^{-3} $PM_{2.5}$ by wind direction and wind speed; C) regional back-trajectory analysis of Wildfire period depicting origin of air-masses associated with exceeding 50 µg m^{-3} PM_{10} and 25 µg m^{-3} $PM_{2.5}$ (red/blue regions indicate highest/lowest probabilities); D) daily mean concentration of PM_{10} (black) and $PM_{2.5}$ (blue); E) daily mean (solid line) and hourly maximum (point) concentrations. Dashed lines on D) and E) depict periods of Wildfire (orange) and Reference (black) HVAC sampling (n = 120 days). (For interpretation of the references to colour in this figure legend, the reader is referred to the Web version of this article.)

air-mass trajectories suggest that these PM-rich plumes originated from fires south/south-west of Sydney along the eastern and south-eastern coastline, especially the $PM_{2.5}$ fraction (Fig. 1C). There was evidence for a secondary region located north/north-east of Sydney that contributed mostly to elevated concentrations of PM_{10} (Fig. 1C). However polar plot analyses indicate that this source was relatively minor (Fig. 1B). These results are consistent with documented fire cases presented here (Fig. 1A) and by Li et al. (2021), with smoke plumes cloaking the east and south-eastern coastline and extending across the Tasman Sea (Li et al., 2021).

Generally, over the four-month Wildfire period, daily concentrations of PM_{10} and $PM_{2.5}$ were 34.4 ± 2.2 and 16.6 ± 1.5 µg m^{-3} respectively (mean ± standard error (se); Fig. 1D), with maximum hourly concentrations of up to 854.3 (PM_{10}) and 533.5 ($PM_{2.5}$) µg m^{-3} (Fig. 1E). During non-wildfire Reference conditions, daily concentrations were 2–3 times lower ($p = 0.001$) at 18.3 ± 0.6 µg m^{-3} PM_{10} and 6.0 ± 0.3 µg m^{-3} $PM_{2.5}$ (Fig. 1D). While occasional spikes of up to 81.8 µg m^{-3} occurred (Fig. 1E), these concentrations were not sustained over any 24-h mean period. Fine particles during the Wildfire period comprised 38.1 % (median, q_1–q_3 31.9–50.0) of airborne PM_{10} mass. This was elevated compared to Reference conditions (32.1 %, 27.9–35.7; $p = 0.001$) and the equivalent months before (2018–2019: 33.8 %, 33.0–35.1; $p = 0.014$) and after (2021–2022: 31.0 %, 30.9–31.5; $p = 0.001$) this study, demonstrating that the 2019–2020 plumes were especially enriched with fine, hazardous particles.

Given the HVAC units collected distant and proximate sources of particulates, the Wildfire PM captured and analysed in this study is likely of mixed pyrogenic and urban origin. This is supported by an ensemble of meteorological variables ($p > 0.05$; Fig. S2) and traffic counts ($p = 0.342$; Table S4), which indicate that there was no significant change in local conditions between study periods (see Fig. S2 and Table S4 in the Supplementary Material).

3.2. Impact of wildfires on particle size and morphology

While most particles recovered were within the PM_{10} size fraction for both study periods (>95 %; Table 1), the size distribution of Wildfire samples were significantly finer than the Reference period ($p = 0.001$; Fig. 2), with lower CMDs and a higher proportion of $PM_{2.5}$ ($p = 0.001$; Table 1). Approximately 83 % of Wildfire particles were within the

Table 1
Particle size metrics of Wildfire (n = 21) and Reference (n = 12) PM (mean ± se). Significant PERMANOVA ($P_{(p\text{-}aov)}$) comparisons are denoted by stars (***$p \leq 0.001$; **$p \leq 0.01$; *$p < 0.05$), where ns indicates non-significant ($p > 0.05$). Bold values denote finer particle metrics.

Metric	Wildfire	Reference	$P_{(p\text{-}aov)}$
Proportion of particle number by size fraction (%)			
$PM_{0.1}$	0.0 ± 0.0	0.0 ± 0.0	ns
$PM_{0.1\text{-}1}$	**54.6 ± 1.0**	39.1 ± 1.8	***
PM_1	**54.6 ± 1.0**	39.1 ± 1.8	***
$PM_{2.5}$	**83.0 ± 0.7**	66.9 ± 1.8	***
PM_{10}	**99.5 ± 0.1**	96.8 ± 0.4	***
Count median diameter by size fraction (nm)			
$CMD_{0.1}$	78.0 ± 7.4	58.2 ± 8.6	ns
$CMD_{0.1\text{-}1}$	511.2 ± 2.7	**494.9 ± 5.7**	**
CMD_1	511.2 ± 2.7	**494.9 ± 5.7**	**
$CMD_{2.5}$	**712.2 ± 10.6**	819.4 ± 39.9	**
CMD_{10}	**886.0 ± 22.9**	1403.4 ± 87.8	***
CMD	**892.1 ± 23.1**	1484.8 ± 96.7	***

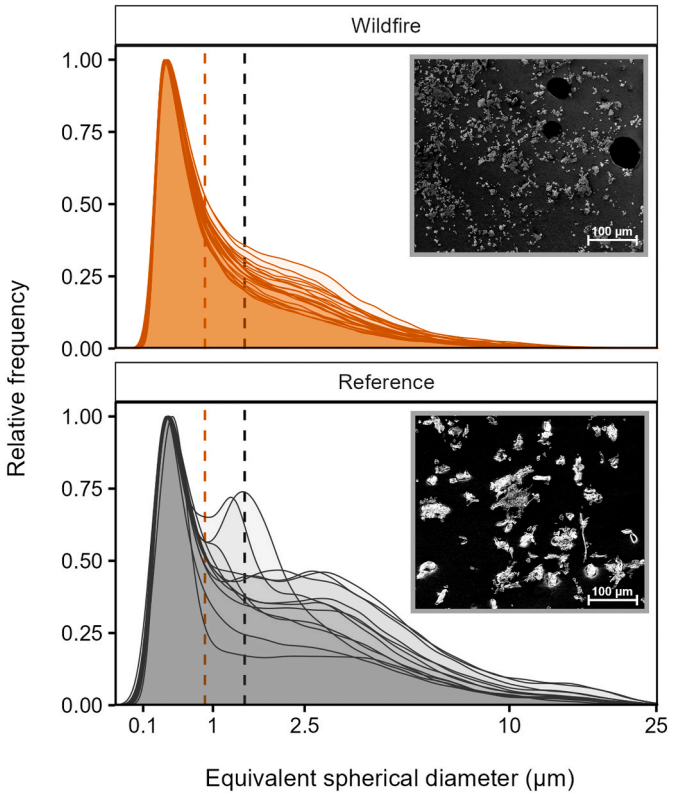

Fig. 2. Particle number size distributions of Wildfire (n = 21) and Reference (n = 12) PM. Individual solid lines depict replicates, where dashed lines denote the mean count median diameters for the Wildfire (orange) and Reference (black) periods. SEM images show the size and morphology of PM sample composites. Overall size distributions differed significantly between study periods (two-sample z-test: $p = 0.001$). Wildfire filters collected from the two buildings did not differ (two-sample z-test: $p = 0.240$). (For interpretation of the references to colour in this figure legend, the reader is referred to the Web version of this article.)

$PM_{2.5}$ fraction, compared to only 67 % in the Reference period. These samples featured CMDs of 892.1 ± 23.1 and 1484.8 ± 96.7 nm, respectively. Given that both biomass and fossil fuel combustion emit fine particles (Reid et al., 2005; Sparks and Wagner, 2021; Wu and Boor, 2021), this increase in $PM_{2.5}$ may be a result of Sydney's distance from the fires (Fig. 1A), with coarser particles settling out faster than fine PM along the smoke plumes' trajectory (Arimoto et al., 1997). Alternatively, prolonged exposure to heavily polluted air could have differentially enhanced the fine PM trapping efficiency of the Wildfire HVAC filters, generating a stronger clogging effect compared to the less polluted Reference filters. This potential effect was analysed independently and found to be negligible (Supplementary Material, Text S2), and thus the differences found here between the two study periods remain valid.

Previous observations indicate that wildfire PM consists mainly of $PM_{0.1\text{-}1}$, with log-normal number size distributions and finer particles relative to ambient conditions (Alonso-Blanco et al., 2012; Okoshi et al., 2014; Reid et al., 2005; Sparks and Wagner, 2021). Wildfire PM in this study was also log-normally distributed (Fig. 2) and featured a higher proportion of $PM_{0.1\text{-}1}$ than the Reference samples ($p = 0.001$; Table 1). However, the CMDs observed for this fraction ($CMD_{0.1\text{-}1}$) were larger than previous aged wildfire smoke observations (511 vs 120–340 nm; Table 1) (Alonso-Blanco et al., 2012; Okoshi et al., 2014; Reid et al., 2005). Furthermore, while particles as small as 21.5 nm were detected by flow cytometry (confirmed by SEM), the abundance of ultrafine PM was extremely rare in both study periods (up to 0.002 %; Table 1). Electron microscopy detected finer and more spherical particles during the Wildfire period (Fig. 2). Observations of residential MERV11 filters during a smoke episode showed particle morphology and chemistry similar to wildfire-generated tar balls (Sparks and Wagner, 2021). Enhanced sphericity is consistent with the photochemical aging of smoke plumes, where processes such as coating by secondary aerosols and gas-to-particle conversion produce more physically rounded particles compared with fresh emissions (Giordano et al., 2015; Pósfai et al., 2003; Ruellan et al., 1999).

There are many possible reasons for the differences observed in particle sizes between wildfire studies, such as: concentration-enhanced coagulation of particles during atmospheric transport (especially given that emissions were record-breaking) (Hirsch and Koren, 2021); greater contributions from coarse mineral particles entrained during strong wildfire-driven winds and thunderstorms (Peterson et al., 2018, 2021); and <1 µm particle losses due to constraints of the FF approach. The latter may include: fine PM passing through the HVAC filter; agglomeration of fine PM to coarser particles during dust cake formation or within the 25 µm pre-screen; and strong particle-to-surface forces preventing retrieval of fine PM from the filter mesh (Mahdavi et al., 2021; Mahdavi and Siegel, 2020). Existing observations during the 2019–2020 Wildfires in Tumbarumba, Australia (464 km south-west of HVAC sampling site) found median particle diameters of 280–500 nm associated with PM_{10} in smoke (Li et al., 2021). Given the above, it is likely that constraints of the FF approach prevented the retrieval of a portion of particles in the PM_1 fraction, though to what extent is unknown. Nonetheless, the relative impact of the Wildfires on particle size relative to the Reference period remained evident.

3.3. Potentially toxic elements: chemical composition and solubility

The potentially toxic fingerprint of Wildfire PM was distinct compared to the Reference period, varying in both the centre ($p = 0.001$) and spread ($p = 0.026$) of clusters in the PCA (Fig. 3). Broadly, Wildfire PM was characterised by higher concentrations of acidic ions, including SO_4^{2-}-S and NO_3^--N ($p = 0.001$; Fig. 3 and Table 2). Both study periods displayed varying concentrations of Cl^- and Na^+ (Fig. 3), though concentrations were higher in Wildfire samples ($p = 0.001$; Table 2). During Reference conditions, Cl^- displayed strong associations with NO_3^--N ($r = 0.99$), Na^+ (0.98) and SO_4^{2-}-S (0.92), indicative of aged sea salt (Zhang and Chan, 2023) from adjacent waters (Fig. 1A). However, the disparity between vector positions in the PCA indicates that Na^+ did not solely explain the variation in Cl^- (Fig. 3), with weaker (but still strong) associations in Wildfire PM ($r = 0.92$ vs 0.98). Further, Cl^- displayed low-moderate correlations with SO_4^{2-}-S (0.41 vs 0.92) and NO_3^--N (0.13 vs 0.99), indicating little association with aged sea salt.

Compared with ambient emissions, these results suggest an alternative source of SO_4^{2-}-S and NO_3^--N during the fires, and an additional, minor source of Cl^-. This is consistent with observations during the

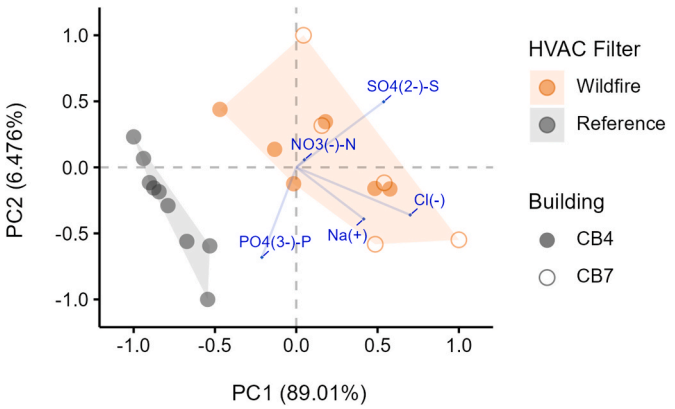

Fig. 3. Principal Components Analysis (PCA) biplot depicting differences in the potentially toxic fingerprint of Wildfire (orange, n = 12) and Reference (black, n = 9) PM. Points closer together have more similar mass composition and vice versa. Blue vectors represent the direction and magnitude of elements driving the greatest differences amongst samples. Study periods differed significantly in both the centre (PERMANOVA: $p = 0.001$) and spread (PERMDISP: $p = 0.026$) of PCA clusters. Wildfire filters collected from the two buildings (closed/open circles) did not differ (PERMANOVA: $p = 0.227$; PERMDISP: $p = 0.821$). (For interpretation of the references to colour in this figure legend, the reader is referred to the Web version of this article.)

Table 2
Potentially toxic ions (and Na^+) in Wildfire (n = 12) and Reference (n = 9) PM (median, q_1–q_3). Significant differences between periods (PERMANOVA ($P_{(p\text{-aov})}$) are denoted by stars (***$p \leq 0.001$; **$p \leq 0.01$; *$p < 0.05$), where ns indicates non-significant ($p > 0.05$). Bold values denote higher median concentrations. LOD = limit of detection.

	Wildfire	Reference	$P_{(p\text{-aov})}$
mg g^{-1}			
Cl^-	**34.7** (30.5–45.5)	15.8 (15-3–21.1)	***
Na^+	**24.5** (21.9–31.9)	11.5 (8.8–15.5)	***
NO_3^--N	**2.4** (2.3–4.1)	1.2 (1.0–1.6)	***
PO_4^{3-}-P	1.4 (0.7–5.5)	**10.4** (9.9–12.4)	***
SO_4^{2-}-S	**20.4** (15.6–28.5)	4.7 (4.1–6.2)	***
μg g^{-1}			
F^-	**334.9** (230.3–384.8)	<LOD	***
NH_4^+-N	0.0 (0.0–216.3)	**466.2** (0.0–478.5)	*
NO_2^--N	0.0 (0.0–13.6)	**19.2** (16.1–21.7)	*

2019–2020 Black Summer, which document chlorine perturbations due to oxidized organics and sulfates (Bernath et al., 2022; Solomon et al., 2023) and nitrate-enriched smoke (Perron et al., 2022; Simmons et al., 2022). Furthermore, it is well established that Cl, NO_x and SO_2 are gaseous species formed during combustion (Akagi et al., 2011; Benedict et al., 2017), and that the aging of particles during transport serves to increase inorganics through secondary aerosol production (Akagi et al., 2011; Li et al., 2015; Pósfai et al., 2003). These species tend to be ubiquitous wildfire by-products across the globe, including in Canada, south-east Asia, and the United States (Adam et al., 2021; Harper et al., 2019). In contrast, PM captured during the Reference period was enriched with PO_4^{3-}-P ($p = 0.001$; Fig. 3 and Table 2), likely due to greater contributions from fossil fuel combustion (Wang et al., 2015). By mass, these three PTEs (SO_4^{2-}-S, PO_4^{3-}-P, NO_3^--N) were the major drivers of variation between the two study periods given their orthogonal positioning relative to clusters in the PCA (Fig. 3). This is consistent with historical observations in Western Australia, where oxalate, nitrate and sulfate were the most reliable tracers for biomass burning in 2015–2018 (Strzelec et al., 2020a). The first two principal components explained 95.5 % of the variability amongst samples, indicating that these differences were well represented. The remaining PTEs were generally less abundant with lower mass contributions to the PCA (<5 %), however many exhibited significant shifts between the two study periods (Tables 2 and 3).

Interestingly, Wildfire PM contained substantially more F^- than Reference samples ($p = 0.001$; Table 2). The primary source of F^- emissions in Australia tend to be industrial (Department of the Environment, 2015), however recent evaluations have shown global biomass burning to be a major source of F-containing particles, comparable to and often exceeding that of coal combustion and other anthropogenic sources (Jayarathne et al., 2014). While F^- was not targeted in other Black Summer monitoring, increases in F^- concentration have been related to distal fires east and north-west of Poland (Lewandowska et al., 2013). Reports of NH_4^+ demonstrated 1.7-fold enrichment (Perron et al., 2022) and significant correlations ($R^2 = 0.87$) with Carbon Monoxide (biomass burning tracer) (Simmons et al., 2022). Comparatively, we detected almost no NH_4^+-N and little NO_2^--N (Table 2). Further, these elements were both higher during Reference conditions (though effects were marginal; $p = 0.029$ and 0.045 respectively; Table 2). Given that wildfires emit significant quantities of NH_3 (Campbell et al., 2022) and the degree of NO_3^--N enrichment observed in this study (2-fold vs 1.5-fold in (Perron et al., 2022)), this discrepancy is likely due to differences in oxidative particle formation during atmospheric transport, where NH_3 and NO_2 were converted more efficiently to NO_3 compounds (Lindaas et al., 2021).

Particulate matter arriving in Sydney during the Wildfires displayed comparatively low concentrations of most trace elements relative to the Reference period, including fraction(s) of Cu, Cd, Hg, Ni and Pb (Table 3). This could be expected given these elements are major atmospheric by-products of non-ferrous metal production, coal and oil combustion, and vehicular traffic worldwide (Grigoratos and Martini, 2015; Pacyna and Pacyna, 2001). Meanwhile, Wildfire PM contained higher concentrations of particulate Co and Sb, and both fractions of Mn (Table 3). Correlation analyses with Pb (a common marker for anthropogenic activity) suggest a predominantly urban source of Co and Mn in the Reference samples ($r = 0.91$ and 0.97) and an alternative source during the Wildfires (0.21 and 0.10). Co and Mn in Australian aerosols are often associated with mineral dust when found offshore (Strzelec et al., 2020a,b), indicating that these PTEs probably originated from soil that was entrained during strong pyrogenic winds (Wagner et al., 2018). This is consistent with previous wildfire smoke observations in Sydney (Isley and Taylor, 2020). Interestingly, Sb exhibited moderate associations with Pb in both study periods, indicative of a mixed-urban source, but had distinct associations with the other PTEs: in Reference PM, Sb was associated with Co ($r = 0.79$ vs −0.07), Mn (0.70 vs −0.40) and Pb (0.66 vs 0.55), whereas Wildfire samples were associated with Cu (0.95 vs 0.13), Cr (0.79 vs −0.31) and Pb (0.55 vs 0.66). Despite ranking seventh for global production (Britt and Senior, 2021), Sb remains unreported in Australian wildfire monitoring, yet has significant potential for remobilisation from current and historical mining sites (Telford et al., 2009), waste-disposal sites (Wilson et al., 2014) and shooting ranges (Sanderson et al., 2014).

While prior observations during the Black Summer Wildfires also detected Mn enrichment in aerosols and sediment deposits (Barros et al., 2022; Perron et al., 2022), Co and Sb were not targeted by these studies, nor did we detect enrichment of other PTEs like As, Cu, Cr, Ni, Pb and Zn (Barros et al., 2022; Biswas et al., 2021; Perron et al., 2022). This is likely due to differences in sampling technique, where airborne samples are influenced by pollutant loading (which was exceptionally high during the Wildfires) and the current study assessed differences on an equal-mass basis. Therefore, we emphasise that our results are likely to be conservative when assessing the impact of wildfires on PTE exposure. Future studies should aim to pair FF with HVAC systems information to estimate atmospheric PTE exposures (Mahdavi et al., 2021) and include airborne sampling techniques where possible for methodological comparisons.

The solubility of Wildfire PTEs were either equal to (Cd, Cr, Mn, Pb, Zn; $p \geq 0.076$) or lower than (Co, Cu, Ni, Sb; $p \leq 0.01$) the Reference

Table 3
Potentially toxic trace elements in Wildfire (n = 12) and Reference (n = 9) PM (median, q_1–q_3). Significant PERMANOVA ($P_{(p\text{-}aov)}$) and PERMDISP ($P_{(p\text{-}disp)}$) comparisons are denoted by stars (***$p \leq 0.001$; **$p \leq 0.01$; *$p < 0.05$), where ns indicates non-significant ($p > 0.05$). Bold values denote higher median concentrations/solubilities and wider quartile ranges (solubility only). LOD = limit of detection.

	Dissolved			Particulate			Solubility			
	Wildfire	Reference	$P_{(p\text{-}aov)}$	Wildfire	Reference	$P_{(p\text{-}aov)}$	Wildfire	Reference	$P_{(p\text{-}aov)}$	$P_{(p\text{-}disp)}$
$\mu g\ g^{-1}$							%			
As	<LOD	<LOD	ns	<LOD	<LOD	ns	<LOD	<LOD	ns	ns
Be	<LOD	<LOD	ns	<LOD	<LOD	ns	<LOD	<LOD	ns	ns
Cd	0.1 (0–0.1)	0.2 (0.1–0.2)	ns	0.3 (0.2–0.4)	**1.7** (1.5–2.2)	***	17.2 **(5.4–25.4)**	6.5 (4.3–8.0)	ns	**
Co	1.2 (0.9–1.6)	1.2 (1.1–1.5)	ns	**13.6** (13.0–16.4)	7.9 (7.0–8.8)	***	7.0 (5.3–10.3)	**13.3** (12.2–15.0)	**	ns
Cr	0 (0–0)	0 (0–0)	ns	119.6 (93.0–135.6)	147.6 (108.7–160.2)	ns	0 (0–0)	0 (0–0)	ns	ns
Cu	39.8 (27.5–47.9)	**83.7** (80–100.9)	***	775.7 (593.9–1011.3)	742.5 (653.9–772.8)	ns	5.2 (3.6–5.7)	**10.1** (9.4–12.0)	***	ns
Hg	7.2 (2.9–13.5)	13.2 (7.6–25.6)	ns	45.8 (33.3–75.7)	**848.6** (243.4–1132.1)	***	**12.2 (4.7–25.5)**	1.0 (0.8–10.1)	*	*
Mn	**108.0** (85.5–163.8)	28.6 (27.8–31.8)	***	**870.3** (719.7–986.5)	303.4 (290.1–349.3)	***	10.1 **(8.2–18.2)**	8.5 (7.7–9.0)	ns	*
Ni	3.4 (2.9–5.9)	**38.1** (33.9–42.2)	***	63.9 (52.1–70.8)	**222.9** (139.3–237.8)	***	5.8 (4.8–8.2)	**15.7** (12.8–19.6)	***	ns
Pb	0.1 (0.1–0.3)	**0.4** (0.4–0.5)	**	68.2 (59.0–80.5)	**129.6** (120.8–143.2)	**	0.2 (0.1–0.4)	0.3 (0.3–0.4)	ns	ns
Sb	1.7 (1.2–3.2)	2.7 (2.5–2.9)	ns	**64.1** (50.0–90.1)	17.4 (15.7–29.5)	***	2.7 (2.0–4.4)	**12.7 (9.3–15.6)**	***	***
Zn	199.8 (123.8–479.2)	283.8 (163.8–293.9)	ns	3699.4 (2618.6–3944.6)	3734.7 (3495.0–3795.2)	ns	4.2 (3.2–13.3)	7.1 (4.2–8.7)	ns	ns

period, except for Hg ($p = 0.025$) (Table 3). Given that both anthropogenic and biomass combustion sources are associated with high trace element solubilities (Baker et al., 2006; Mahowald et al., 2018), a differential enhancement of Hg is likely due to high-temperature induced volatilisation and emission of anthropogenic deposits on vegetation, litter, and soil (Howard et al., 2019). This is consistent with observations of wildfire ash, where Hg had the highest solubility of all elements analysed (Harper et al., 2019). While the central tendency of PTE solubilities were generally higher in Reference PM, the upper range and level of dispersion was either similar (Co, Cr, Cu, Ni, Pb, Zn; $p \geq 0.196$) or greater (Cd, Hg, Mn) than Reference PM for all trace elements except Sb (Table 3). This was expected given that HVAC filters received substantial contributions from a variety of smoke plume populations, sampling emissions of different source locations and characteristics (e.g., organic/inorganic particle matrix; moisture content; reactions with co-emitted organics, oxidisers, acidic species; photochemical processing and mixing; plume age, etc.) (Andreae, 2019; Baker and Jickells, 2006; Desboeufs et al., 2005; Hsu et al., 2010; Longo et al., 2016; Yang et al., 2023).

The PTEs detected in this study have a wide range of toxic effects at relatively low concentrations on diverse biota. In humans, ions like F^- are extremely permeable across biological membranes, where their inhalation even in low concentrations elicits acute airway inflammation (Lund et al., 1999), and epithelial lung cell apoptosis at high concentrations (Refsnes et al., 2003). Similarly, trace elements such as Mn and Cu are major contributors to oxidative stress (Fujitani et al., 2017), while soluble forms of Hg can rapidly absorb and spread to all major organs in the human body (Park and Zheng, 2012). Upon their deposition, anions (mainly SO_4^{2-} and NO_3^-) may acidify surface waters and forest-floor soils (Battles et al., 2014; Lawrence et al., 1995; Lydersen et al., 2014) impacting acid-sensitive organisms, whilst PTEs like F^- and Mn may elicit direct toxicity in receiving environments (Alexakis, 2020; Golding et al., 2023; Wang et al., 2022). These impacts vary in their scale, from cellular (e.g., oxidative stress; DNA degradation, etc.) to organism level (impaired development, behaviours, and function), to populations (prolific growth of algae; mass fish kills) up to widescale ecosystem disturbances (trace element mobilisation; reduced nutrient storage; altered trophic flows and food availability) (Ding et al., 2022; Fornasiero, 2001; Leduc et al., 2013; McNulty and Newman, 1961; Monteith et al., 2007; Muniz, 1990; Wang et al., 2022). These impacts tend to be long-lived given that many trace elements are not readily biodegradable, persisting in the organism and environment for decades, even after removing the source (Gall et al., 2015).

4. Conclusions

The 2019–2020 Black Summer Wildfires were a major remote source of particle pollution in Sydney, especially fires originating on the south and south-east coast of Australia. Throughout HVAC sampling, daily mean PM concentrations were 2–3 times higher than the Reference period and exceeded the national standards on 19 % of days across the four-month sampling window. The wildfires were a significant source of $PM_{2.5}$ mass, comprising 31.9–50.0 % (q_1–q_3) of PM_{10} compared to only 27.9–35.7 % during Reference conditions. In this study, we show that particles collected during the Wildfires were significantly finer and more spherical than ambient urban PM. Particle number size distributions were finer, with 83.0 ± 0.7 versus 66.9 ± 1.8 % of particles <2.5 μm, and CMDs of 892.1 ± 23.1 and 1484.8 ± 96.7 nm, respectively. On an equal-mass basis, aged mixed wildfire-urban particles were a major source of acidic ions, including SO_4^{2-S} (20.4 vs 4.7 mg g^{-1}) and NO_3^--N (2.4 vs 1.2 mg g^{-1}). Wildfire samples were also enriched with other PTEs, including Cl^- (34.7 vs 15.8 mg g^{-1}), F^- (334.9 μg g^{-1} vs < LOD), dissolved Mn (108.0 vs 28.6 μg g^{-1}), and particulate forms of Mn (870.3 vs 303.4 μg g^{-1}), Co (13.6 vs 7.9 μg g^{-1}), and Sb (64.1 vs 17.4 μg g^{-1}). Wildfire PM featured higher Hg solubility (12.1 vs 1.0 %) and displayed a greater range of Hg (q_1–q_3 4.7–25.5 vs 0.8–10.1 %), Cd (5.4–25.4 vs 4.3–8.0 %), and Mn (8.2–18.2 vs 7.7–9.0 %) solubilities. Together, Wildfire PM displayed significant potential for toxicity given these elements are highly mobile, bioavailable, and persistent in the environment. Therefore, inhalation and deposition of this material had a high probability of negative impacts in the Sydney human population and on surrounding ecosystems.

Funding

This work was supported by the Faculty of Science and Climate Change Cluster at the University of Technology Sydney (UTS) through provision of operation funds and equipment, as well as the NSW Department of Planning and Environment (DPE) through in-kind contributions of expertise and the provision of consumables. RLG was

supported by an Australian Government Research Training Program Scholarship at UTS.

CRediT authorship contribution statement

Raissa L. Gill: Writing – review & editing, Writing – original draft, Visualization, Methodology, Investigation, Formal analysis, Data curation, Conceptualization. **Robert Fleck:** Writing – review & editing, Methodology, Investigation, Conceptualization. **Ky Chau:** Writing – review & editing, Investigation. **Mika T. Westerhausen:** Writing – review & editing, Methodology, Investigation. **Thomas E. Lockwood:** Writing – review & editing, Methodology, Investigation. **Jake P. Violi:** Writing – review & editing, Investigation. **Peter J. Irga:** Writing – review & editing, Conceptualization. **Martina A. Doblin:** Writing – review & editing, Supervision, Conceptualization. **Fraser R. Torpy:** Writing – review & editing, Supervision, Methodology, Conceptualization.

Declaration of competing interest

The authors declare that they have no known competing financial interests or personal relationships that could have appeared to influence the work reported in this paper.

Data availability

Data will be made available on request.

Acknowledgements

The authors acknowledge the Climate and Atmospheric Science Branch from the NSW Department of Planning and Environment (DPE) for provision of atmospheric PM and meteorological data, and Transport for NSW for the provision of traffic count data. The authors gratefully acknowledge the NOAA Air Resources Laboratory (ARL) for the provision of the HYSPLIT transport and dispersion model and READY website (ready.noaa.gov) used in this publication. We acknowledge the Department of Climate Change, Energy, the Environment and Water as well as the following providers for their contributions to the National Indicative Aggregated Fire Extent Datasets: NSW Rural Fire Service, Northern Australian Fire Information (NAFI), QLD Fire and Emergency Service, QLD Department of Environment and Science, SA Country Fire Service, SA Department for Environment and Water, Tasmanian Fire Service, TAS Department of Primary Industry, Parks, Water and Environment, VIC Department of Environment, Land, Water and Planning, WA Department of Biodiversity, Conservation and Attractions. For the symbols used to assemble the graphical abstract, we acknowledge Tracey Saxby and Jane Hawkey from the Integration and Application Network (ian.umces.edu/media-library) for the following artworks: Estuary 3D: braided river mouth; Climate change: wildfire; Urban: city 1; Industry 2; Sediment. The Sediment symbol was modified by cropping it from the original. All symbols are licensed under a Creative Commons Attribution-ShareAlike 4.0 International (CC BY-SA 4.0) license (creativecommons.org/licenses/by-sa/4.0). Finally, the authors would like to acknowledge the three anonymous reviewers for their insightful feedback which improved the manuscript.

Appendix A. Supplementary data

Supplementary data to this article can be found online at https://doi.org/10.1016/j.envpol.2024.123306.

References

Adam, M.G., Tran, P.T.M., Bolan, N., Balasubramanian, R., 2021. Biomass burning-derived airborne particulate matter in Southeast Asia: a critical review. J. Hazard Mater. 407, 124760 https://doi.org/10.1016/j.jhazmat.2020.124760.

Aguilera, R., Corringham, T., Gershunov, A., Benmarhnia, T., 2021. Wildfire smoke impacts respiratory health more than fine particles from other sources: observational evidence from Southern California. Nat. Commun. 12 https://doi.org/10.1038/s41467-021-21708-0.

Akagi, S.K., Yokelson, R.J., Wiedinmyer, C., Alvarado, M.J., Reid, J.S., Karl, T., Crounse, J.D., Wennberg, P.O., 2011. Emission factors for open and domestic biomass burning for use in atmospheric models. Atmos. Chem. Phys. 11, 4039–4072. https://doi.org/10.5194/acp-11-4039-2011.

Alavy, M., Siegel, J.A., 2020. In-situ effectiveness of residential HVAC filters. Indoor Air 30, 156–166. https://doi.org/10.1111/ina.12617.

Aldersley, A., Murray, S.J., Cornell, S.E., 2011. Global and regional analysis of climate and human drivers of wildfire. Sci. Total Environ. 409, 3472–3481. https://doi.org/10.1016/j.scitotenv.2011.05.032.

Alexakis, D.E., 2020. Suburban areas in flames: dispersion of potentially toxic elements from burned vegetation and buildings. Estimation of the associated ecological and human health risk. Environ. Res. 183, 109153 https://doi.org/10.1016/j.envres.2020.109153.

Alonso-Blanco, E., Calvo, A.I., Fraile, R., Castro, A., 2012. The influence of wildfires on aerosol size distributions in rural areas. Sci. World J. 2012, 1–13. https://doi.org/10.1100/2012/735697.

Andreae, M.O., 2019. Emission of trace gases and aerosols from biomass burning – an updated assessment. Atmos. Chem. Phys. 19, 8523–8546. https://doi.org/10.5194/acp-19-8523-2019.

Arimoto, R., Ray, B.J., Lewis, N.F., Tomza, U., Duce, R.A., 1997. Mass-particle size distributions of atmospheric dust and the dry deposition of dust to the remote ocean. J. Geophys. Res. Atmos. 102, 15867–15874. https://doi.org/10.1029/97JD00796.

Arnholt, A.T., Evans, B., 2021. BSDA: Basic Statistics and Data Analysis. https://cran.r-project.org/. (Accessed 22 March 2023).

Australian Bureau of Statistics, 2023. Regional Population. https://www.abs.gov.au/. (Accessed 22 March 2023).

Baker, A.R., Jickells, T.D., 2006. Mineral particle size as a control on aerosol iron solubility. Geophys. Res. Lett. 33, L17608 https://doi.org/10.1029/2006GL026557.

Baker, A.R., Jickells, T.D., Witt, M., Linge, K.L., 2006. Trends in the solubility of iron, aluminium, manganese and phosphorus in aerosol collected over the Atlantic Ocean. Mar. Chem. 98, 43–58. https://doi.org/10.1016/j.marchem.2005.06.004.

Barros, T.L., Bracewell, S.A., Mayer-Pinto, M., Dafforn, K.A., Simpson, S.L., Farrell, M., Johnston, E.L., 2022. Wildfires cause rapid changes to estuarine benthic habitat. Environ. Pollut. 308, 119571 https://doi.org/10.1016/j.envpol.2022.119571.

Battles, J.J., Fahey, T.J., Driscoll, C.T., Blum, J.D., Johnson, C.E., 2014. Restoring soil calcium reverses forest decline. Environ. Sci. Technol. Lett. 1, 15–19. https://doi.org/10.1021/ez400033d.

Beck, H.E., Zimmermann, N.E., McVicar, T.R., Vergopolan, N., Berg, A., Wood, E.F., 2018. Present and future köppen-geiger climate classification maps at 1-km resolution. Sci. Data 5, 1–12. https://doi.org/10.1038/sdata.2018.214.

Benedict, K.B., Prenni, A.J., Carrico, C.M., Sullivan, A.P., Schichtel, B.A., Collett, J.L., 2017. Enhanced concentrations of reactive nitrogen species in wildfire smoke. Atmos. Environ. 148, 8–15. https://doi.org/10.1016/j.atmosenv.2016.10.030.

Bernath, P., Boone, C., Crouse, J., 2022. Wildfire smoke destroys stratospheric ozone. Science 375, 1292–1295. https://doi.org/10.1126/science.abm5611.

Biswas, T.K., Karim, F., Kumar, A., Wilkinson, S., Guerschman, J., Rees, G., McInerney, P., Zampatti, B., Sullivan, A., Nyman, P., Sheridan, G.J., Joehnk, K., 2021. 2019–2020 Bushfire impacts on sediment and contaminant transport following rainfall in the Upper Murray River catchment. Integr. Environ. Assess. Manag. 17, 1203–1214. https://doi.org/10.1002/ieam.4492.

Boer, M.M., Resco de Dios, V., Bradstock, R.A., 2020. Unprecedented burn area of Australian mega forest fires. Nat. Clim. Change 10, 171–172. https://doi.org/10.1038/s41558-020-0716-1.

Borchers Arriagada, N., Palmer, A.J., Bowman, D.M.J.S., Morgan, G.G., Jalaludin, B.B., Johnston, F.H., 2020. Unprecedented smoke-related health burden associated with the 2019–20 bushfires in eastern Australia, Med. J. Aust 213, 282–283. https://doi.org/10.5694/mja2.50545.

Bowman, D.M.J.S., Kolden, C.A., Abatzoglou, J.T., Johnston, F.H., van der Werf, G.R., Flannigan, M., 2020. Vegetation fires in the Anthropocene. Nat. Rev. Earth Environ. 1, 500–515. https://doi.org/10.1038/s43017-020-0085-3.

Britt, A.F, Senior, A.B, 2021. Australian Resource Reviews: Antimony 2020. https://doi.org/10.11636/9781922446534. Geoscience Australia, Canberra.

Campbell, P.C., Tong, D., Saylor, R., Li, Y., Ma, S., Zhang, X., Kondragunta, S., Li, F., 2022. Pronounced increases in nitrogen emissions and deposition due to the historic 2020 wildfires in the western U.S. Sci. Total Environ. 839, 156130 https://doi.org/10.1016/j.scitotenv.2022.156130.

Carslaw, D.C., Ropkins, K., 2012. openair — an R package for air quality data analysis. Environ. Model. Software 27–28, 52–61. https://doi.org/10.1016/j.envsoft.2011.09.008.

Climate and Atmospheric Science Branch, Department of Planning and Environment, 2023. Air quality monitoring network. NSW Gov. https://www.environment.nsw.gov.au/. (Accessed 22 March 2023).

Cohen, D.D., Atanacio, A.J., Stelcer, E., Garton, D., 2016. Sydney Particle Characterisation Study. Australian Nuclear Science and Technology Organisation, NSW Gov. https://www.environment.nsw.gov.au/. (Accessed 22 March 2023).

Cohen, D.D., Stelcer, E., Garton, D., Crawford, J., 2011. Fine particle characterisation, source apportionment and long-range dust transport into the Sydney Basin: a long term study between 1998 and 2009. Atmos. Pollut. Res. 2, 182–189. https://doi.org/10.5094/APR.2011.023.

Costa, D.L., Dreher, K.L., 1997. Bioavailable transition metals in particulate matter mediate cardiopulmonary injury in healthy and compromised animal models.

Environ. Health Perspect. 105, 1053–1060. https://doi.org/10.1289/ehp.97105s51053.
Department of Climate Change, Energy, the Environment and Water, 2020. Australian Government. National Indicative Aggregated Fire Extent Datasets (NIAFED_20190701_20200622_v20200623). https://www.dcceew.gov.au/. (Accessed 22 March 2023).
Department of the Environment, 2015. National Pollutant Inventory Guide. Australian Government. https://www.dcceew.gov.au/. (Accessed 22 March 2023).
Department of the Environment and Heritage, 2005. National Standards for Criteria Air Pollutants 1 in Australia. https://www.environment.gov.au/. (Accessed 22 March 2023).
Desboeufs, K.V., Sofikitis, A., Losno, R., Colin, J.L., Ausset, P., 2005. Dissolution and solubility of trace metals from natural and anthropogenic aerosol particulate matter. Chemosphere 58, 195–203. https://doi.org/10.1016/j.chemosphere.2004.02.025.
Dev, S., Barnes, D., Kadir, A., Betha, R., Aggarwal, S., 2022. Outdoor and indoor concentrations of size-resolved particulate matter during a wildfire episode in interior Alaska and the impact of ventilation. Air Qual. Atmos. Heal. 15, 149–158. https://doi.org/10.1007/s11869-021-01094-8.
Ding, C., Chen, J., Zhu, F., Chai, L., Lin, Z., Zhang, K., Shi, Y., 2022. Biological toxicity of heavy metal(loid)s in natural environments: from microbes to humans. Front. Environ. Sci. 10, 1–23. https://doi.org/10.3389/fenvs.2022.920957.
Dunnington, D., 2023. ggspatial: Spatial Data Framework for ggplot2. https://cran.r-project.org/. (Accessed 22 March 2023).
Dong, T.T.T., Hinwood, A.L., Callan, A.C., Zosky, G., Stock, W.D., 2017. In vitro assessment of the toxicity of bushfire emissions: a review. Sci. Total Environ. 603–604, 268–278. https://doi.org/10.1016/j.scitotenv.2017.06.062.
Fornasiero, R.B., 2001. Phytotoxic effects of fluorides. Plant Sci. 161, 979–985. https://doi.org/10.1016/S0168-9452(01)00499-X.
Franzi, L.M., Bratt, J.M., Williams, K.M., Last, J.A., 2011. Why is particulate matter produced by wildfires toxic to lung macrophages? Toxicol. Appl. Pharmacol. 257, 182–188. https://doi.org/10.1016/j.taap.2011.09.003.
Fujitani, Y., Furuyama, A., Tanabe, K., Hirano, S., 2017. Comparison of oxidative abilities of PM2.5 collected at traffic and residential sites in Japan. Contribution of transition metals and primary and secondary aerosols. Aerosol Air Qual. Res. 17, 574–587. https://doi.org/10.4209/aaqr.2016.07.0291.
Gall, J.E., Boyd, R.S., Rajakaruna, N., 2015. Transfer of heavy metals through terrestrial food webs: a review. Environ. Monit. Assess. 187, 201. https://doi.org/10.1007/s10661-015-4436-3.
Gaudichet, A., Echalar, F., Chatenet, B., Quisefit, J.P., Malingre, G., Cachier, H., Buat-Menard, P., Artaxo, P., Maenhaut, W., 1995. Trace elements in tropical African savanna biomass burning aerosols. J. Atmos. Chem. 22, 19–39. https://doi.org/10.1007/BF00708179.
Giordano, M., Espinoza, C., Asa-Awuku, A., 2015. Experimentally measured morphology of biomass burning aerosol and its impacts on CCN ability. Atmos. Chem. Phys. 15, 1807–1821. https://doi.org/10.5194/acp-15-1807-2015.
Golding, L.A., Binet, M.T., Adams, M.S., Hochen, J., Humphrey, C.A., Price, G.A.V., Reichelt-Brushett, A.J., Salmon, M., Stauber, J.L., 2023. Acute and chronic toxicity of manganese to tropical adult coral (Acropora millepora) to support the derivation of marine manganese water quality guideline values. Mar. Pollut. Bull. 194, 115242 https://doi.org/10.1016/j.marpolbul.2023.115242.
Grigoratos, T., Martini, G., 2015. Brake wear particle emissions: a review. Environ. Sci. Pollut. Res. 22, 2491–2504. https://doi.org/10.1007/s11356-014-3696-8.
Hanley, J.T., Ensor, D.S., Smith, D.D., Sparks, L.E., 1994. Fractional aerosol filtration efficiency of in-duct ventilation air cleaners. Indoor Air 4, 169–178. https://doi.org/10.1111/j.1600-0668.1994.t01-1-00005.x.
Harper, A.R., Santin, C., Doerr, S.H., Froyd, C.A., Albini, D., Otero, X.L., Viñas, L., Pérez-Fernández, B., 2019. Chemical composition of wildfire ash produced in contrasting ecosystems and its toxicity to Daphnia magna. Int. J. Wildland Fire 28, 726–737. https://doi.org/10.1071/WF18200.
Hirsch, E., Koren, I., 2021. Record-breaking aerosol levels explained by smoke injection into the stratosphere. Science 371, 1269–1274. https://doi.org/10.1126/science.abe1415.
Howard, D., Macsween, K., Edwards, G.C., Desservettaz, M., Guérette, E.A., Paton-Walsh, C., Surawski, N.C., Sullivan, A.L., Weston, C., Volkova, L., Powell, J., Keywood, M.D., Reisen, F., Mick, C.P.(, Meyer, 2019. Investigation of mercury emissions from burning of Australian eucalypt forest surface fuels using a combustion wind tunnel and field observations. Atmos. Environ. 202, 17–27. https://doi.org/10.1016/j.atmosenv.2018.12.015.
Hsu, S.-C., Wong, G.T.F., Gong, G.-C., Shiah, F.-K., Huang, Y.-T., Kao, S.-J., Tsai, F., Candice Lung, S.-C., Lin, F.-J., Lin, I.-I., Hung, C.-C., Tseng, C.-M., 2010. Sources, solubility, and dry deposition of aerosol trace elements over the East China Sea. Mar. Chem. 120, 116–127. https://doi.org/10.1016/j.marchem.2008.10.003.
Huang, Y., Wu, S., Kaplan, J.O., 2015. Sensitivity of global wildfire occurrences to various factors in the context of global change. Atmos. Environ. 121, 86–92. https://doi.org/10.1016/j.atmosenv.2015.06.002.
Isley, C.F., Taylor, M.P., 2020. Atmospheric remobilization of natural and anthropogenic contaminants during wildfires. Environ. Pollut. 267, 115400 https://doi.org/10.1016/j.envpol.2020.115400.
Jayarathne, T., Stockwell, C.E., Yokelson, R.J., Nakao, S., Stone, E.A., 2014. Emissions of fine particle fluoride from biomass burning. Environ. Sci. Technol. 48, 12636–12644. https://doi.org/10.1021/es502933j.
Johnston, F.H., Borchers-Arriagada, N., Morgan, G.G., Jalaludin, B., Palmer, A.J., Williamson, G.J., Bowman, D.M.J.S., 2021. Unprecedented health costs of smoke-related PM2.5 from the 2019–20 Australian megafires. Nat. Sustain. 4, 42–47. https://doi.org/10.1038/s41893-020-00610-5.
Kassambara, A., 2020. ggpubr: 'ggplot2' Based Publication Ready Plots. https://cran.r-project.org/. (Accessed 22 March 2023).
Kanakidou, M., Seinfeld, J.H., Pandis, S.N., Barnes, I., Dentener, F.J., Facchini, M.C., Van Dingenen, R., Ervens, B., Nenes, A., Nielsen, C.J., Swietlicki, E., Putaud, J.P., Balkanski, Y., Fuzzi, S., Horth, J., Moortgat, G.K., Winterhalter, R., Myhre, C.E.L., Tsigaridis, K., Vignati, E., Stephanou, E.G., Wilson, J., 2005. Organic aerosol and global climate modelling: a review. Atmos. Chem. Phys. 5, 1053–1123. https://doi.org/10.5194/acp-5-1053-2005.
Lawrence, G.B., David, M.B., Shortle, W.C., 1995. A new mechanism for calcium loss in forest-floor soils. Nature 378, 162–165. https://doi.org/10.1038/378162a0.
Leduc, A.O.H.C., Munday, P.L., Brown, G.E., Ferrari, M.C.O., 2013. Effects of acidification on olfactory-mediated behaviour in freshwater and marine ecosystems: a synthesis. Philos. Trans. R. Soc. B Biol. Sci. 368, 20120447 https://doi.org/10.1098/rstb.2012.0447.
Lewandowska, A., Falkowska, L., Jóźwik, J., 2013. Factors determining the fluctuation of fluoride concentrations in PM_{10} aerosols in the urbanized coastal area of the Baltic Sea (Gdynia, Poland). Environ. Sci. Pollut. Res. 20, 6109–6118. https://doi.org/10.1007/s11356-013-1592-2.
Li, C., Ma, Z., Chen, J., Wang, X., Ye, X., Wang, L., Yang, X., Kan, H., Donaldson, D.J., Mellouki, A., 2015. Evolution of biomass burning smoke particles in the dark. Atmos. Environ. 120, 244–252. https://doi.org/10.1016/j.atmosenv.2015.09.003.
Li, M., Shen, F., Sun, X., 2021. 2019−2020 Australian bushfire air particulate pollution and impact on the South Pacific Ocean. Sci. Rep. 11, 12288 https://doi.org/10.1038/s41598-021-91547-y.
Lindaas, J., Pollack, I.B., Calahorrano, J.J., O'Dell, K., Garofalo, L.A., Pothier, M.A., Farmer, D.K., Kreidenweis, S.M., Campos, T., Flocke, F., Weinheimer, A.J., Montzka, D.D., Tyndall, G.S., Apel, E.C., Hills, A.J., Hornbrook, R.S., Palm, B.B., Peng, Q., Thornton, J.A., Permar, W., Wielgasz, C., Hu, L., Pierce, J.R., Collett, J.L., Sullivan, A.P., Fischer, E.V., 2021. Empirical insights into the fate of ammonia in western U.S. wildfire smoke plumes. J. Geophys. Res. Atmos. 126 https://doi.org/10.1029/2020JD033730.
Longo, A.F., Feng, Y., Lai, B., Landing, W.M., Shelley, R.U., Nenes, A., Mihalopoulos, N., Violaki, K., Ingall, E.D., 2016. Influence of atmospheric processes on the solubility and composition of iron in Saharan dust. Environ. Sci. Technol. 50, 6912–6920. https://doi.org/10.1021/acs.est.6b02605.
Lund, K., Refsnes, M., Sandstrom, T., Søstrand, P., Schwarze, P., Boe, J., Kongerud, J., 1999. Increased CD3 positive cells in bronchoalveolar lavage fluid after hydrogen fluoride inhalation. Scand. J. Work. Environ. Health 25, 326–334. https://doi.org/10.5271/sjweh.442.
Lydersen, E., Høgberget, R., Moreno, C.E., Garmo, Ø.A., Hagen, P.C., 2014. The effects of wildfire on the water chemistry of dilute, acidic lakes in southern Norway. Biogeochemistry 119, 109–124. https://doi.org/10.1007/s10533-014-9951-8.
Mahdavi, A., Siegel, J.A., 2020. Extraction of dust collected in HVAC filters for quantitative filter forensics. Aerosol Sci. Technol. 54, 1282–1292. https://doi.org/10.1080/02786826.2020.1774492.
Mahdavi, A., Dingle, J., Chan, A.W.H., Siegel, J.A., 2021. HVAC filtration of particles and trace metals: airborne measurements and the evaluation of quantitative filter forensics. Environ. Pollut. 271, 116388 https://doi.org/10.1016/j.envpol.2020.116388.
Mahowald, N.M., Hamilton, D.S., Mackey, K.R.M.M., Moore, J.K., Baker, A.R., Scanza, R.A., Zhang, Y., 2018. Aerosol trace metal leaching and impacts on marine microorganisms. Nat. Commun. 9, 2614. https://doi.org/10.1038/s41467-018-04970-7.
McNulty, I.B., Newman, D.W., 1961. Mechanism (s) of fluoride induced chlorosis. Plant Physiol. 36, 385–388. https://doi.org/10.1104/pp.36.4.385.
Miller, F.J., Gardner, D.E., Graham, J.A., Lee, R.E., Wilson, W.E., Bachmann, J.D., 1979. Size considerations for establishing a standard for inhalable particles. J. Air Pollut. Control Assoc. 29, 610–615. https://doi.org/10.1080/00022470.1979.10470831.
Monteith, D.T., Stoddard, J.L., Evans, C.D., de Wit, H.A., Forsius, M., Høgåsen, T., Wilander, A., Skjelkvåle, B.L., Jeffries, D.S., Vuorenmaa, J., Keller, B., Kopácek, J., Vesely, J., 2007. Dissolved organic carbon trends resulting from changes in atmospheric deposition chemistry. Nature 450, 537–540. https://doi.org/10.1038/nature06316.
Muniz, I.P., 1990. Freshwater acidification: its effects on species and communities of freshwater microbes, plants and animals. Proc. R. Soc. Edinburgh. Sect. B. Biol. Sci. 97, 227–254. https://doi.org/10.1017/S0269727000005364.
Nemmar, A., Hoet, P.H.M., Vanquickenborne, B., Dinsdale, D., Thomeer, M., Hoylaerts, M.F., Vanbilloen, H., Mortelmans, L., Nemery, B., 2002. Passage of inhaled particles into the blood circulation in humans. Circulation 105, 411–414. https://doi.org/10.1161/hc0402.104118.
Nolan, R.H., Boer, M.M., Resco de Dios, V., Caccamo, G., Bradstock, R.A., 2016. Large-scale, dynamic transformations in fuel moisture drive wildfire activity across southeastern Australia. Geophys. Res. Lett. 43, 4229–4238. https://doi.org/10.1002/2016GL068614.
Okoshi, R., Rasheed, A., Chen Reddy, G., McCrowey, C.P., Curtis, D.B., 2014. Size and mass distributions of ground-level sub-micrometer biomass burning aerosol from small wildfires. Atmos. Environ. 89, 392–402. https://doi.org/10.1016/j.atmosenv.2014.01.024.
Oksanen, J., Blanchet, G.F., Friendly, M., Kindt, R., Legendre, P., McGlinn, D., Minchin, P.R., O'Hara, R.B., Simpson, G.L., Solymos, P., Stevens, M.H.H., Szoecs, E., Wagner, H., 2022. vegan: Community Ecology Package. https://cran.r-project.org/. (Accessed 22 March 2023).
Pacyna, J.M., Pacyna, E.G., 2001. An assessment of global and regional emissions of trace metals to the atmosphere from anthropogenic sources worldwide. Environ. Rev. 9, 269–298. https://doi.org/10.1139/a01-012.

Park, J.D., Zheng, W., 2012. Human exposure and health effects of inorganic and elemental mercury. J. Prev. Med. Public Heal. 45, 344–352. https://doi.org/10.3961/jpmph.2012.45.6.344.

Paytan, A., Mackey, K.R.M., Chen, Y., Lima, I.D., Doney, S.C., Mahowald, N., Labiosa, R., Post, A.F., 2009. Toxicity of atmospheric aerosols on marine phytoplankton. Proc. Natl. Acad. Sci. USA 106, 4601–4605. https://doi.org/10.1073/pnas.0811486106.

Pebesma, E., 2018. Simple Features for R: standardized support for spatial vector data. R J 10, 439–446. https://doi.org/10.32614/RJ-2018-009.

Pechony, O., Shindell, D.T., 2010. Driving forces of global wildfires over the past millennium and the forthcoming century. Proc. Natl. Acad. Sci. U.S.A. 107, 19167–19170. https://doi.org/10.1073/pnas.1003669107.

Perron, M.M.G., Meyerink, S., Corkill, M., Strzelec, M., Proemse, B.C., Gault-Ringold, M., Sanz Rodriguez, E., Chase, Z., Bowie, A.R., 2022. Trace elements and nutrients in wildfire plumes to the southeast of Australia. Atmos. Res. 270, 106084 https://doi.org/10.1016/j.atmosres.2022.106084.

Peterson, D.A., Campbell, J.R., Hyer, E.J., Fromm, M.D., Kablick, G.P., Cossuth, J.H., DeLand, M.T., 2018. Wildfire-driven thunderstorms cause a volcano-like stratospheric injection of smoke. Npj Clim. Atmos. Sci. 1, 30. https://doi.org/10.1038/s41612-018-0039-3.

Peterson, D.A., Fromm, M.D., McRae, R.H.D., Campbell, J.R., Hyer, E.J., Taha, G., Camacho, C.P., Kablick, G.P., Schmidt, C.C., DeLand, M.T., 2021. Australia's Black Summer pyrocumulonimbus super outbreak reveals potential for increasingly extreme stratospheric smoke events. Npj Clim. Atmos. Sci. 4, 1–16. https://doi.org/10.1038/s41612-021-00192-9.

Pinkerton, K.E., Green, F.H.Y., Saiki, C., Vallyathan, V., Plopper, C.G., Gopal, V., Hung, D., Bahne, E.B., Lin, S.S., Ménache, M.G., Schenker, M.B., 2000. Distribution of particulate matter and tissue remodeling in the human lung. Environ. Health Perspect. 108, 1063–1069. https://doi.org/10.1289/ehp.001081063.

Pósfai, M., Simonics, R., Li, J., Hobbs, P.V., Buseck, P.R., 2003. Individual aerosol particles from biomass burning in southern Africa: 1. Compositions and size distributions of carbonaceous particles. J. Geophys. Res. Atmos. 108 https://doi.org/10.1029/2002JD002291.

R Core Team, 2022. R: A Language and Environment for Statistical Computing. Version 4.2.1. https://www.r-project.org/. (Accessed 1 December 2022).

Refsnes, M., Schwarze, P.E., Holme, J.A., Låêg, M., 2003. Fluoride-induced apoptosis in human epithelial lung cells (A549 cells): role of different G protein-linked signal systems. Hum. Exp. Toxicol. 22, 111–123. https://doi.org/10.1191/0960327103ht322oa.

Reid, C.E., Brauer, M., Johnston, F.H., Jerrett, M., Balmes, J.R., Elliott, C.T., 2016. Critical review of health impacts of wildfire smoke exposure. Environ. Health Perspect. 124, 1334–1343. https://doi.org/10.1289/ehp.1409277.

Reid, J.S., Koppmann, R., Eck, T.F., Eleuterio, D.P., 2005. A review of biomass burning emissions part II: intensive physical properties of biomass burning particles. Atmos. Chem. Phys. 5, 799–825. https://doi.org/10.5194/acp-5-799-2005.

Riley, M.L., Kirkwood, J., Jiang, N., Ross, G., Scorgie, Y., 2020. Air quality monitoring in NSW: From long term trend monitoring to integrated urban services. Air Qual. Clim. Change 54 (1), 44–51. https://doi.org/10.3316/informit.078202598997117.

Rolph, G., Stein, A., Stunder, B., 2017. Real-time Environmental Applications and Display sYstem: READY. Eviron. Model. Softw. 95, 210–228. https://doi.org/10.1016/j.envsoft.2017.06.025.

Ruellan, S., Cachier, H., Gaudichet, A., Masclet, P., Lacaux, J.P., 1999. Airborne aerosols over central Africa during the experiment for regional sources and sinks of oxidants (EXPRESSO). J. Geophys. Res. Atmos. 104, 30673–30690. https://doi.org/10.1029/1999JD900804.

Sanderson, P., Naidu, R., Bolan, N., 2014. Ecotoxicity of chemically stabilised metal(loid)s in shooting range soils. Ecotoxicol. Environ. Saf. 100, 201–208. https://doi.org/10.1016/j.ecoenv.2013.11.003.

Simmons, J.B., Paton-Walsh, C., Mouat, A.P., Kaiser, J., Humphries, R.S., Keywood, M., Griffith, D.W.T., Sutresna, A., Naylor, T., Ramirez-Gamboa, J., 2022. Bushfire smoke plume composition and toxicological assessment from the 2019–2020 Australian Black Summer. Air Qual. Atmos. Heal. 15, 2067–2089. https://doi.org/10.1007/s11869-022-01237-5.

Solomon, S., Stone, K., Yu, P., Murphy, D.M., Kinnison, D., Ravishankara, A.R., Wang, P., 2023. Chlorine activation and enhanced ozone depletion induced by wildfire aerosol. Nature 615, 259–264. https://doi.org/10.1038/s41586-022-05683-0.

Sparks, T.L., Wagner, J., 2021. Composition of particulate matter during a wildfire smoke episode in an urban area. Aerosol Sci. Technol. 55, 734–747. https://doi.org/10.1080/02786826.2021.1895429.

Stabler, B., 2022. shapefiles: Read and Write ESRI Shapefiles. https://cran.r-project.org/. (Accessed 22 March 2023).

Stein, A.F., Draxler, R.R., Rolph, G.D., Stunder, B.J.B., Cohen, M.D., Ngan, F., 2015. NOAA's HYSPLIT Atmospheric Transport and Dispersion Modeling System. Bull. Am. Meteorol. Soc. 96, 2059–2077. https://doi.org/10.1175/BAMS-D-14-00110.1.

Stephens, B., Siegel, J.A., 2012. Comparison of test methods for determining the particle removal efficiency of filters in residential and light-commercial central HVAC systems. Aerosol Sci. Technol. 46, 504–513. https://doi.org/10.1080/02786826.2011.642825.

Strzelec, M., Proemse, B.C., Barmuta, L.A., Gault-Ringold, M., Desservettaz, M., Boyd, P.W., Perron, M.M.G., Schofield, R., Bowie, A.R., 2020a. Atmospheric trace metal deposition from natural and anthropogenic sources in western Australia. Atmosphere 11, 474. https://doi.org/10.3390/atmos11050474.

Strzelec, M., Proemse, B.C., Gault-Ringold, M., Boyd, P.W., Perron, M.M.G., Schofield, R., Ryan, R.G., Ristovski, Z.D., Alroe, J., Humphries, R.S., Keywood, M.D., Ward, J., Bowie, A.R., 2020b. Atmospheric trace metal deposition near the great Barrier Reef, Australia. Atmosphere 11, 390. https://doi.org/10.3390/atmos11040390.

Sumner, M., 2021. ozmaps: Australia Maps. https://cran.r-project.org/. (Accessed 22 March 2023).

Tang, W., Llort, J., Weis, J., Perron, M.M.G., Basart, S., Li, Z., Sathyendranath, S., Jackson, T., Sanz Rodriguez, E., Proemse, B.C., Bowie, A.R., Schallenberg, C., Strutton, P.G., Matear, R., Cassar, N., 2021. Widespread phytoplankton blooms triggered by 2019–2020 Australian wildfires. Nature 597, 370–375. https://doi.org/10.1038/s41586-021-03805-8.

Telford, K., Maher, W., Krikowa, F., Foster, S., Ellwood, M.J., Ashley, P.M., Lockwood, P.V., Wilson, S.C., 2009. Bioaccumulation of antimony and arsenic in a highly contaminated stream adjacent to the Hillgrove Mine, NSW, Australia. Environ. Chem. 6, 133. https://doi.org/10.1071/EN08097.

Transport for NSW, 2023. Traffic Volume Viewer. NSW Gov. https://www.transport.nsw.gov.au/. (Accessed 4 November 2023).

Uria-Tellaetxe, I., Carslaw, D.C., 2014. Conditional bivariate probability function for source identification. Environ. Model. Software 59, 1–9. https://doi.org/10.1016/j.envsoft.2014.05.002.

van der Velde, I.R., van der Werf, G.R., Houweling, S., Maasakkers, J.D., Borsdorff, T., Landgraf, J., Tol, P., van Kempen, T.A., van Hees, R., Hoogeveen, R., Veefkind, J.P., Aben, I., 2021. Vast CO_2 release from Australian fires in 2019–2020 constrained by satellite. Nature 597, 366–369. https://doi.org/10.1038/s41586-021-03712-y.

Wagner, R., Jähn, M., Schepanski, K., 2018. Wildfires as a source of airborne mineral dust – revisiting a conceptual model using large-eddy simulation (LES). Atmos. Chem. Phys. 18, 11863–11884. https://doi.org/10.5194/acp-18-11863-2018.

Wang, R., Balkanski, Y., Boucher, O., Ciais, P., Peñuelas, J., Tao, S., 2015. Significant contribution of combustion-related emissions to the atmospheric phosphorus budget. Nat. Geosci. 8, 48–54. https://doi.org/10.1038/ngeo2324.

Wang, X., Liu, B.-L., Gao, X.-Q., Fang, Y.-Y., Zhang, X.-H., Cao, S.-Q., Zhao, K.-F., Wang, F., 2022. Effect of long-term manganese exposure on oxidative stress, liver damage and apoptosis in grouper Epinephelus moara ♀ × Epinephelus lanceolatus ♂. Front. Mar. Sci. 9, 721–733. https://doi.org/10.3389/fmars.2022.1000282.

Ward, M., Tulloch, A.I.T., Radford, J.Q., Williams, B.A., Reside, A.E., Macdonald, S.L., Mayfield, H.J., Maron, M., Possingham, H.P., Vine, S.J., O'Connor, J.L., Massingham, E.J., Greenville, A.C., Woinarski, J.C.Z., Garnett, S.T., Lintermans, M., Scheele, B.C., Carwardine, J., Nimmo, D.G., Lindenmayer, D.B., Kooyman, R.M., Simmonds, J.S., Sonter, L.J., Watson, J.E.M., 2020. Impact of 2019–2020 mega-fires on Australian fauna habitat. Nat. Ecol. Evol. 4, 1321–1326. https://doi.org/10.1038/s41559-020-1251-1.

Wegesser, T.C., Pinkerton, K.E., Last, J.A., 2009. California wildfires of 2008: coarse and fine particulate matter toxicity. Environ. Health Perspect. 117, 893–897. https://doi.org/10.1289/ehp.0800166.

Weschler, C.J., Nazaroff, W.W., 2010. SVOC partitioning between the gas phase and settled dust indoors. Atmos. Environ. 44, 3609–3620. https://doi.org/10.1016/j.atmosenv.2010.06.029.

Wickham, H., 2016. ggplot2: Elegant Graphics for Data Analysis. Springer-Verlag, New York. https://ggplot2.tidyverse.org/. (Accessed 22 March 2023).

Wickham, H., François, R., Henry, L., Müller, K., 2022. dplyr: A Grammar of Data Manipulation. https://cran.r-project.org/. (Accessed 22 March 2023).

Wilson, S.C., Tighe, M., Paterson, E., Ashley, P.M., 2014. Food crop accumulation and bioavailability assessment for antimony (Sb) compared with arsenic (As) in contaminated soils. Environ. Sci. Pollut. Res. 21, 11671–11681. https://doi.org/10.1007/s11356-014-2577-5.

Wu, T., Boor, B.E., 2021. Urban aerosol size distributions: a global perspective. Atmos. Chem. Phys. 21, 8883–8914. https://doi.org/10.5194/acp-21-8883-2021.

Xu, Y., Liang, Y., Urquidi, J.R., Siegel, J.A., 2015. Semi-volatile organic compounds in heating, ventilation, and air-conditioning filter dust in retail stores. Indoor Air 25, 79–92. https://doi.org/10.1111/ina.12123.

Yang, J., Ma, L., He, X., Au, W.C., Miao, Y., Wang, W.-X., Nah, T., 2023. Measurement report: abundance and fractional solubilities of aerosol metals in urban Hong Kong – insights into factors that control aerosol metal dissolution in an urban site in South China. Atmos. Chem. Phys. 23, 1403–1419. https://doi.org/10.5194/acp-23-1403-2023.

Zhang, R., Chan, C.K., 2023. Simultaneous formation of sulfate and nitrate via co-uptake of SO_2 and NO_2 by aqueous NaCl droplets: combined effect of nitrate photolysis and chlorine chemistry. Atmos. Chem. Phys. 23, 6113–6126. https://doi.org/10.5194/acp-23-6113-2023.